THE JOURNAL OF PHYSICAL CHEMISTRY B

ARTICLE

pubs.acs.org/JPCB

Investigation of Model Membrane Disruption Mechanism by Melittin using Pulse Electron Paramagnetic Resonance Spectroscopy and Cryogenic Transmission Electron Microscopy

Michal Gordon-Grossman,[†] Herbert Zimmermann,[∥] Sharon G. Wolf,[§] Yechiel Shai,[‡] and Daniella Goldfarb*[,†]

[†]Department of Chemical Physics, [‡]Department of Biological Chemistry, and [§]Department of Chemical Research Support, The Weizmann Institute of Science, Rehovot, Israel 76100

[∥]Max-Planck Institute for Medical Research, Heidelberg, Germany

Supporting Information

ABSTRACT: Studies of membrane peptide interactions at the molecular level are important for understanding essential processes such as membrane disruption or fusion by membrane active peptides. In a previous study, we combined several electron paramagnetic resonance (EPR) techniques, particularly continuous wave (CW) EPR, electron spin echo envelope modulation (ESEEM), and double electron−electron resonance (DEER) with Monte Carlo (MC) simulations to probe the conformation, insertion depth, and orientation with respect to the membrane of the membrane active peptide melittin. Here, we combined these EPR techniques with cryogenic transmission electron microscopy (cryo-TEM) to examine the effect of the peptide/phospholipid (P/PL) molar ratio, in the range of 1:400 to 1:25, on the membrane shape, lipids packing, and peptide orientation and penetration. Large unilamellar vesicles (LUVs) of DPPC/PG (7:3 dipalmitoylphosphatidylcholine/egg phosphatidylglycerol) were used as model membranes. Spin-labeled peptides were used to probe the peptide behavior whereas spin-labeled phspholipids were used to examine the membrane properties. The cryo-TEM results showed that melittin causes vesicle rupture and fusion into new vesicles with ill-defined structures. This new state was investigated by the EPR methods. In terms of the peptide, CW EPR showed decreased mobility, and ESEEM revealed increased insertion depth as the P/PL ratio was raised. DEER measurements did not reveal specific aggregates of melittin, thus excluding the presence of stable, well-defined pore structures. In terms of membrane properties, the CW EPR reported reduced mobility in both polar head and alkyl chain regions with increasing P/PL. ESEEM measurements showed that, as the P/PL ratio increased, a small increase in water content in the PL headgroup region took place and no change was observed in the alkyl chains part close to the hydrophilic region. In terms of lipid local density, opposite behavior was observed for the polar head and alkyl chain regions with increasing P/PL; while the DPPC density increased in the polar head region, it decreased in the alkyl chain region. These results are consistent with disruption of the lipid order and segregation of the PL constituents of the membrane as a consequence of the melittin binding. This work further demonstrates the applicability and potential of pulse EPR techniques for the study of peptide−membrane interactions.

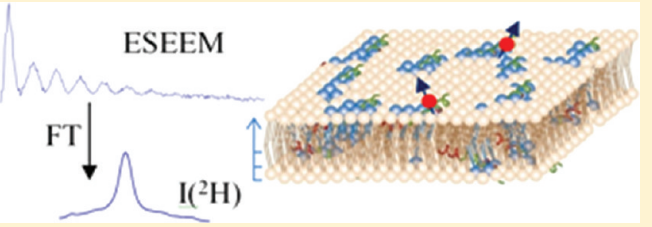

INTRODUCTION

Studies of membrane−peptide interactions at the molecular level are important for understanding essential processes such as membrane disruption or fusion by membrane active peptides. Such studies include identification and characterization of the peptide−membrane assemblies that form as the peptides adsorb on the membrane. Peptide−membrane assemblies have been investigated extensively by a number of physical experimental techniques, including oriented circular dichroism (OCD),[1] solid-state NMR,[2−5] Raman spectroscopy,[6] and X-ray diffraction,[7] each having its advantages and disadvantages in terms of resolution and sensitivity.

Another prominent method is electron paramagnetic resonance (EPR) spectroscopy and its variants. It relies on site-directed spin labeling (SDSL) of the peptide or phospholipids (PL). Traditionally such studies rely mostly on line shape analysis of the continuous wave (CW) EPR spectrum that gives information on ordering, mobility, and polarity.[8,9] In addition, line broadening and increased relaxation rates due to the presence of paramagnetic quenchers provide solvent accessibility and insertion depth in membranes.[8,10−12] This approach is well-established and can reveal the secondary structure and the general location and orientation of the peptide relative to the membrane.[8,13] In addition, pulse EPR techniques such as distance measurements by double electron−electron

Received: July 27, 2011
Revised: November 17, 2011
Published: November 17, 2011

resonance (DEER) and electron spin echo envelope modulations (ESEEM) designed to probe peptide conformations, exposure to water, and insertion into membrane have become more abundant in the past decade.[14−19]

Recently,[20] to this collection of techniques has been added an approach that combines several EPR techniques, particularly CW EPR, ESEEM, and DEER, combined with Monte Carlo (MC) simulation to probe the peptide conformation, side chain mobility, insertion depth, and orientation with respect to the model membrane. This approach was demonstrated on melittin, the major component of honeybee (*Apis mellifera*) venom[21,22] interacting with large unilamellar vesicles (LUVs) of 7:3 DPPC/PG (dipalmitoylphosphatidylcholine/egg phosphatidylglycerol) as model membranes. Melittin is an amphipathic, highly cationic (+5) 26 residue peptide that is often used as a model to study peptide−membrane interactions.[23,24] The orientation and penetration depth of melittin in the model membrane were determined by ESEEM measurements.[20,25] These were carried out on melittin mutants, singly labeled with nitroxides by SDSL,[8] that were added to LUVs to either LUVs containing specifically deuterated lipids suspended in H_2O or nondeuterated LUVs suspended in D_2O. In these experiments, we exploited the dipolar interaction between the spin label and ^2H nuclei at specific locations in the lipid molecules or in the water. This interaction is manifested as modulations in the echo decay with a frequency equal to the ^2H Larmor frequency, while the modulation depth is related to the number of ^2H nuclei and their distances from the spin.[26] The peptide conformation was deduced from DEER intramolecular distance measurements between two spin labels in doubly labeled melittin mutants.[27] In addition to the experimental work, MC simulations were carried out to derive the peptide−membrane energetics and average conformation of the native peptide and mutants serving as models to the spin-labeled peptides. A good agreement was obtained between the experimental results and the MC simulations for the distance distributions, side chain mobility, and orientation with respect to the membrane surface. These data showed that for P/PL = 200 and a negatively charged membrane, melittin adsorbs on the surface of the membrane as a monomeric amphipathic helix, and solvent exposed residues were identified, in agreement with earlier studies.[24] Overall, this study gave a detailed molecular level characterization of the peptide in a negatively charged model membrane system.

The mechanism of peptides active membrane in general, and melittin in particular, requires a threshold peptide concentration for activation that depends on membrane composition.[24,28] The architecture of melittin induced pores was studied extensively, and a few models such as "barrel-stave", "carpet", and "toroidal pore" were suggested for its mechanism.[23,29−31] Here, we further explore the applicability of the integrated CW and pulse EPR approach for the characterization of the peptide in the membrane, specifically focusing on the effect of the melittin/phospholipid ratio on the peptide orientation, its aggregation state within the membrane, and the associated changes that occur in the membrane properties. Here, in addition to spin-labeled peptides, we have used spin-labeled phospholipid molecules, with the spin label attached at different positions along the lipid, enabeling us to probe changes in the membrane properties[32] particularly their packing, in different depths of the membrane. In addition to the EPR measurements that provide molecular level information and directly probe the peptide interaction with the lipid molecules, we carried out cryogenic transmission electron microscopy (cryo-TEM) measurements. These visualize changes at the mesoscopic level that the model membrane undergoes upon binding melittin. The cryo-TEM results were then correlated with the molecular level information obtained from the EPR measurements yielding a more complete picture of the system.

The cryo-TEM results showed that melittin ruptured the original LUVs, which then underwent fusion, yielding a new equilibrium state of large vesicles with ill-defined shapes. The number of fused vesicles increased with increasing P/PL ratio. It is this new state that was explored by EPR. The EPR findings were consistent with a model where melittin was bound to the membrane surface, and as the P/PL increased, it penetrated deeper into the membrane. While we observed an increase of melittin local concentration on the LUVs with increasing P/PL, as expected, we did not detect any specific, well-defined aggregate structures. This indicates that well-defined pores lined by melittin molecules are not present in the newly formed vesicles. Furthermore, changes of opposite directions in the density of the DPPC lipids were observed in the polar head and in the hydrophobic core. This was interpreted in terms of disorder induced by peptide and lipids segregated to form regions richer with negative PG lipids close to the cationic peptide and other that are rich with DPPC. The implications of these findings in terms of the current available models for melittin action are discussed.

EXPERIMENTAL SECTION

Materials. The PL dipalmitoylphosphatidylcholine (DPPC) (Sigma) and the egg phosphatidylglycerol (PG) (Lipid products) were used as is. 1,2-Dipalmitoyl-3-phosphatidylcholine-d_9, where the methyl groups of the choline at the headgroup are deuterated, (DPPC-d_9) was synthesized as reported earlier, and the isotopic purity was found to be better than 98%.[33] Perdeuterated alkyl chain DPPC (DPPC-d_{62}) was purchased from Avanti Polar Lipids Inc. MTSL (1-oxyl-2, 2, 5, 5-tetramethyl-3-pyrroline-3-methyl) methanethiosulfonate was from Toronto Research Chemicals, 1,2-dipalmitoyl-sn-glycero-3-phospho (TEMPO) choline (HPCSP), and 1-palmitoyl-2-stearoyl-(10-DOXYL)-*sn*-glycero-3-phosphocholine (10PCSP) were purchased from Avanti Polar Lipids Inc. 1-Palmitoyl-2-stearoyl-(5-DOXYL)-*sn*-glycero-3-phosphocholine (5PCSP) was synthesized according to procedure described earlier.[34] Perdeuterated glycerol-d_8 was purchased from Cambridge Isotope Labratories.

Peptide Synthesis, Spin Labeling, Purification, and Sample Preparation. Peptides were synthesized, spin labeled with MTSL, and purified as described earlier.[8] Table 1 lists the peptides prepared and their designations.

Dry phospholipid (PL) mixtures of DPPC/PG (7:3 w/w), DPPC-d_9/PG (7:3 w/w), or DPPC-d_{62}/PG (7:3 w/w) were dissolved in a $CHCl_3$/MeOH mixture (2:1, v/v). Each of the spin-labeled PL, 5PCSP,105PCSP, or HPCSP was added from a stock solution to the phospholipid solution to give 1% by weight. The solvents were evaporated under a nitrogen stream. Lipid suspension was prepared by vortex mixing and sonication of the lipids in phosphate buffer (pH 7.2, 0.1 mM in H_2O or D_2O) to give a final concentration of 5 mg/mL. Once the sample was fully hydrated, large unilamellar vesicles (LUVs) were prepared by extrusion through a polycarbonate filter with a pore size of 0.1 μ with an Avastin LiposoFast extruder.[35] The peptides were added to the LUVs solution to give a total peptide concentration of 0.06, 0.13, 0.25, 0.5, and 1 mM at the corresponding P/PL molar ratios of 1/400, 1/200, 1/100, 1/50, and 1/25. These ratios were

Table 1. Peptide Designations and Sequences[a]

sequence	peptide designation
GIGAVLKVLTTGLPALISWIKRKRQQ	melittin
GIC̲AVLKVLTTGLPALISWIKRKRQQ	mel-C_3
GIGAVLKVLTTGLPC̲LISWIKRKRQQ	mel-C_{15}

[a] C̲ indicates the position of the labeling.

obtained under the assumption of a 100% yield of LUVs. In each sample for ESEEM measurements, where singly labeled melittin has been used, the spin concentration remained constant (0.13 mM). Here, the total concentration of the peptide was changed by adding different amounts of unlabeled melittin to the samples. Exceptions are the samples where the total peptide concentration was 0.06 mM where only labeled peptide was used.

All samples for DEER measurements were prepared in D_2O solutions to extend the phase memory time. There the concentration of the doubly labeled peptide was increased, namely, no unlabeled melittin was used. Samples for DEER and ESEEM measurements were prepared as follows: mixtures of LUVs with peptide were kept on a hot plate at 303 K for 20 min from preparation; thereafter, approximately 40 μL was inserted into an EPR tube (2.7 mm i.d. and 3.7 mm o.d.) and rapidly frozen by insertion into liquid nitrogen. The samples were stored in liquid nitrogen. We note that we have not added any cryo-protectant such as glycerol or sucrose as often done in pulse EPR studies involving model membrantes[17,18,36−39] because we did not want to perturb the system.

Cryo-TEM Measurements. The sample (5 μL) was applied to copper TEM grids coated with lacey carbon (SPI Supplies, West Chester, PA, United States), which had been glow-discharged for 15 s. The samples were blotted and plunged into liquid ethane using a CEVS plunger.[40] Grids were transferred to liquid nitrogen and were observed using low-dose imaging techniques at −178 °C using a Gatan 626 cryoholder, on either an FEI Tecnai T12 or Tecnai Spirit electron microscope at 120 kV. Images were recorded on either a TVIPS F224 camera or an FEI Eagle 2k camera.

EPR Spectroscopy. All CW X-band (9.5 GHz.) measurements were performed at 303 or 130 K on a Bruker ELEXSYS 500 spectrometer, using two of round quartz capillaries (0.6 i.d. × 0.84 o.d.). ESEEM and DEER experiments were carried out on a Bruker ELEXSYS E580 spectrometer (9.5 GHz) at 85 and 50 K, respectively.

The ESEEM experiments were done using the three-pulse pulse sequence $\pi/2$ -τ- $\pi/2$ −T- $\pi/2$ -τ-echo, with a repetition rate of 3 ms and four-step phase cycle.[41] All measurements were performed at a field corresponding to the maximum echo intensity and the $\pi/2$ microwave (mw) pulse length was 16 ns. The τ value was optimized for maximum ^{2}H modulation depth ($\tau = {}^1/_2\ \nu_I \sim 224$ ns, where ν_I is the ^{2}H Larmor frequency).[26] The time interval T was incremented in 20 ns steps starting at 40 ns. The number of accumulations was 30−300 depending on the modulation depth. Fourier transformation of the ESEEM (FT-ESEEM) trace was carried out as follows: after phase correction and normalization, the background decay of the normalized data was removed using a polynomial fit, then the data was apodized with a Hamming window, zero filled to 512 points, and FT and cross-term averaging were performed.[42] All ESEEM traces were treated identically.

We chose the intensity of the ^{2}H peak, $I(^2H)$, in the FT-ESEEM spectrum, as a measure for the modulation depth as described earlier.[25] The ^{2}H peak is composed of a narrow component due to remote deuterium nuclei and a broad component due to water molecules that form H bonds with the NO group.[43] The data analysis in the present study took into account only the narrow spectral constituent.

The constant time four-pulse DEER experiment, $\pi/2\ (\nu_{obs})-\tau_1-\pi(\nu_{obs})-t-\pi(\nu_{pump})-(\tau_1+\tau_2-t)-\pi(\nu_{obs})-\tau_2-$echo was employed[44] with a $+x/-x$ phase cycle on the first pulse and averaging over 25 increments of τ_1 (τ_1 = 400 ns; $\Delta\tau_1$ = 8 ns) to suppress nuclear modulations. The echo was measured as a function of t, while τ_1 and τ_2 were kept constant. The pump frequency, ν_{pump}, was set to the center of the resonator bandwidth, and the static magnetic field was set to the maximum of the nitroxide spectrum at the pump frequency. The observer frequency, ν_{obs}, was set at 60 MHz higher than ν_{pump}. The length of all mw pulses was 32 ns, and the dwell time was 20 ns. Typical numbers of shots per point and scan number were 30 and 15−170, respectively. Accumulation times for the data sets varied from 12 to 48 h. The DEER data were analyzed using the DeerAnalysis program.[45]

RESULTS

Morphology of the LUVs. Cryo-TEM images were obtained for DPPC/PG LUVs without melittin and with melittin at P/PL ratios of 1/200, 1/50, and 1/25. The samples for cryo-TEM and EPR measurements were flash frozen 20 min after melittin addition. It has been reported that melittin action on a membrane takes place at a time much shorter than 20 min,[46] and therefore, what we observe is a new equilibrium state. In the absence of melittin, the LUVs appeared round and smooth with a diameter of approximately 150 nm, as shown in Figure 1a. At P/PL = 1/200, we could already observe a few larger LUVs that did not have a well-defined form like the spheres observed before melittin was added (Figure 1b). As the P/PL ratio increased, some bilayer sheets appeared (Figure 1c), and more LUVs with various sizes and shapes were observed. The shapes of the new vesicles clearly indicate that fusion of LUVs had taken place, as seen in Figure 1c for P/PL of 1/25. An image of a sample frozen only one minute after melittin addition (P/PL = 1/25) is presented in Figure 1d. It shows many disks and completely disrupted LUVs indicating that the addition of melittin actually broke some LUVs. These appear to have merged and rearranged to form the large "fused" vesicles that are observed in samples frozen after 20 min from melittin addition. These results show that the peptide is effective already at a P/PL ratio of 1/200, although the number of perturbed structures observed was lower than at higher P/PL ratios. This implies that the number of melittin molecules per LUV should cross a particular threshold in order to disrupt it. These observations are in agreement with earlier reports of cryo-TEM investigation of DOPC and POPC liposomes in the presence of melittin.[47] There too, ruptured liposomes and open bilayer structures were frequently observed in coexistence with closed liposomes.

DPPC Lipid Mobility and Organization. To follow the effect of melittin on the model membrane, we have introduced spin-labeled phospholipids, 5PCSP, 10PCSP, and HPCSP, and followed changes in their local dynamics as a function of the P/PL ratio through their CW EPR spectra. The EPR spectra were recorded at room temperature, 20 min after the addition of melittin. The spectra of 5PCSP and 10PCSP, presented in Figure 2, show that, as the P/PL ratio increases, A_{max} (defined in Figure 2) increases as well. This indicates a decrease in the mobility of each of the

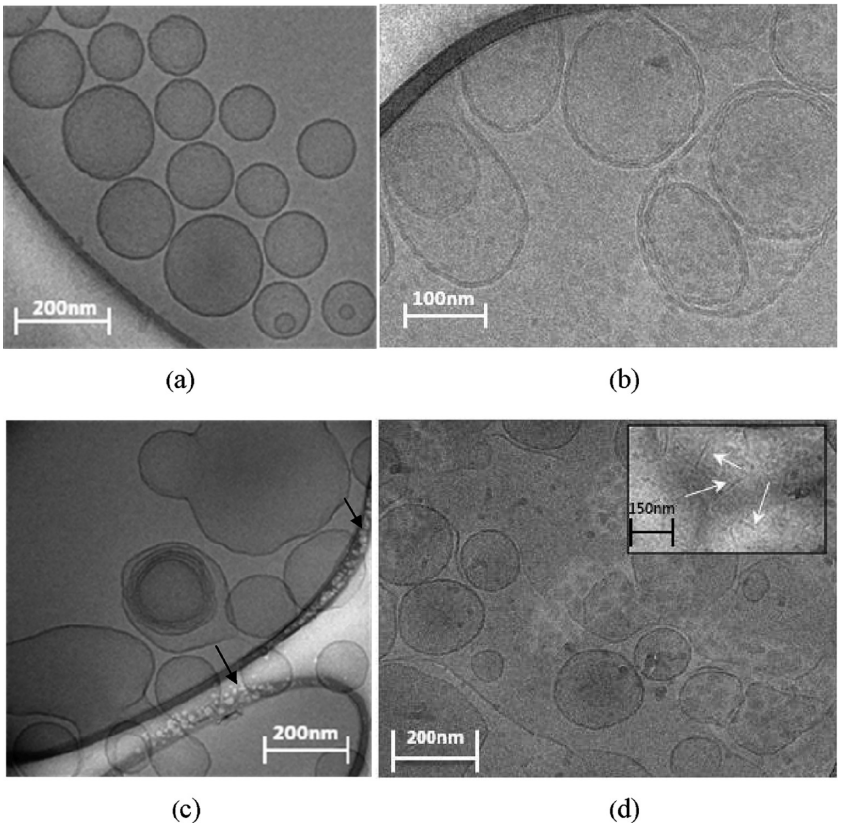

Figure 1. Cryo-TEM images of DPPC/PG LUVs (a) without melittin and with melittin at P/PL ratios of (b) 1/200 and (c) 1/25, captured after approximately 20 min from melittin addition (black arrows indicate irradiation damage), (d) 1/25, captured after approximately 1 min from melittin addition. The white arrows in the insert point on short disks.

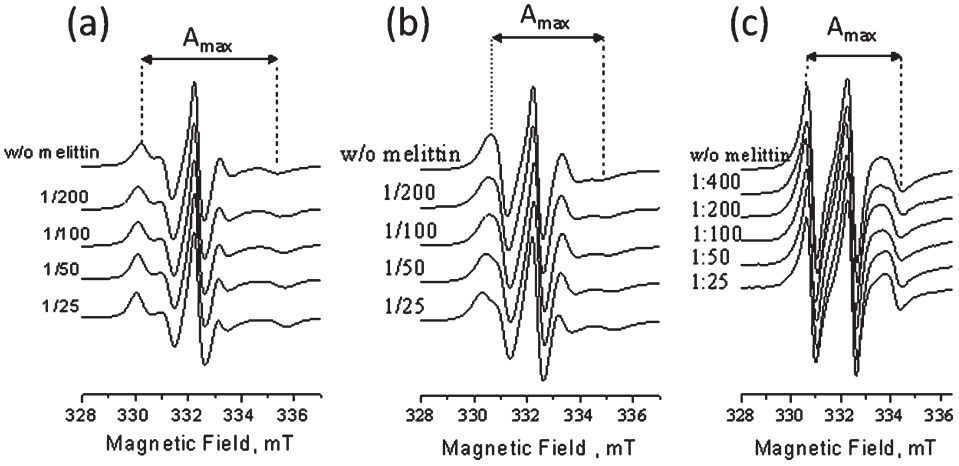

Figure 2. X-band CW EPR spectra (303 K) of (a) 5PCSP, (b) 10PCSP, and (c) HPCSP in the absence and presence of peptides at different P/PL ratios.

spin labels. Comparison of these spectra to the spectra of the LUVs without melittin shows that the spectra with melittin are always broader due to slower tumbling rates, confirming that melittin interacts with the membrane. These observations are in agreement with earlier studies on melittin in DMPC and DTPG bilayers.[28] In contrast to 5PCSP and 10PCSP, no significant changes were observed for the HPCSP probe, which exhibits the highest mobility.

ESEEM measurements on spin-labeled lipids were carried out to monitor variations in the packing and organization of the lipid molecules. This is achieved by monitoring the environment of the spin label through the hyperfine interaction with ^{2}H nuclei on neighboring lipid molecules or in water molecules. HPCSP was used to probe the polar region, whereas 5PCSP and 10PCSP sense different regions within the hydrophobic core of the membrane. Figure 3 presents $I(^2H)$ as a function of P/PL for each lipid spin probe. $I(^2H)$ is the amplitude of the ^{2}H peak in the FT-ESEEM spectrum and is a measure of the modulation depth. A larger $I(^2H)$ value corresponds to higher ^{2}H density around the spin label, namely, the closer and more abundant the ^{2}H nuclei

dx.doi.org/10.1021/jp207159z |J. Phys. Chem. B 2012, 116, 179–188

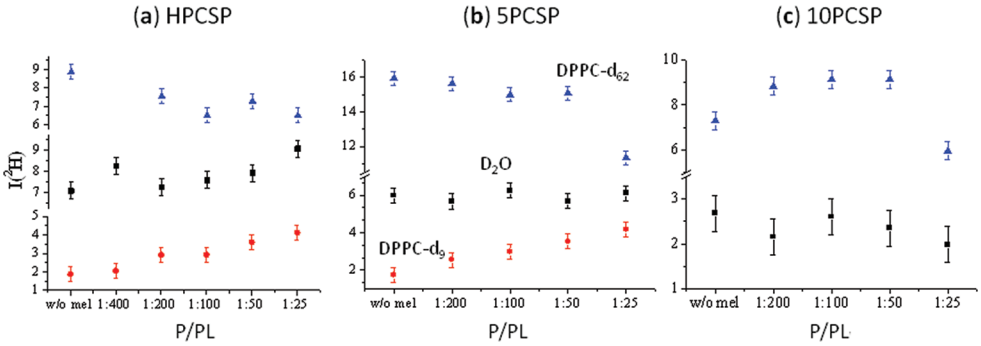

Figure 3. $I(^2H)$ values of (a) HPCSP, (b) 5PCSP, and (c) 10PCSP in the following membranes: DPPC-d_{62}/PG (triangles), DPPC-d_9/PG (circles), and DPPC/PG/D_2O (squares), as a function of P/PL .

are, the larger is $I(^2H)$.[20,25] This analysis is valid when there are no specific interactions between the NO group and the ^2H nuclei, such as ^2H nuclei forming H bonds in D_2O samples. The latter contributes a broad component to the FT-ESEEM signal at the ^2H Larmor frequency.[43] In our analysis of the D_2O solutions, we have removed the contributions of this broad component and focused on the nonspecific interactions with ^2H nuclei. While for both 5PCSP and 10PCSP there is no change in the D_2O $I(^2H)$, some increase was observed for HPCSP with increasing P/PL. This suggests that the water concentration profile in the hydrophobic alkyl chain region of the membrane has not changed as a consequence of the addition of melittin. In contrast, some changes do occur at the polar head region.

We also carried out ESEEM measurements on these PL spin probes within deuterated (DPPC-d_9, DPPC-d_{62}) LUVs, as a function of the P/PL ratios, to probe changes in the lipid organization and composition in the alkyl and headgroup regions. Denser phosphlipids packing at a certain depth of the membrane will be manifested as higher ^2H density in samples containing phosphlipids deuterated at the corresponding positions. The results are displayed in Figure 3. The $I(^2H)$ of HPCSP in DPPC-d_{62}/PG LUVs decreased (see Figure 3a), whereas for DPPC-d_9/PG it increased as the P/PL ratio increased. For DPPC/PG/D_2O, a mild increase was observed. For 5PCSP/DPPC-d_9/PG, an increase of $I(^2H)$ was found upon increasing P/PL ratio whereas for DPPC-d_{62}/PG it decreased and it stayed practically constant for DPPC/PG/D_2O. No modulations were observed for 10PCSP/DPPC-d_9/PG because the label is located too far from the deuterated layer and there is no significant change in DPPC/PG/D_2O. In DPPC-d_{62}/PG, the $I(^2H)$ was initially constant, but at P/PL = 1/25, a significant decrease is observed (Figure 3b, c). The $I(^2H)$ value of 10PCSP/DPPC-d_{62}/PG is lower than for 5PCSP/DPPC-d_{62}/PG, independent of the P/PL, indicating a general lower ^2H density in the end of the alkyl chain region that is consistent with higher disorder.

We summarize these results as follows: increasing P/PL caused (i) an increase in the density of ^2H nuclei of DPPC (DPPC packing) in the polar head region and a decrease in the alkyl chain region and (ii) mild increase of water density in the polar region and no change in the alkyl region.

Melittin Mobility, Orientation, Penetration Depth, and Aggregation State. The effect of P/PL on the peptide mobility was obtained by using a singly labeled melittin, mel-C_{15}, added to LUVs consisting of phospholipids without any spin labels. Figure 4 shows the CW EPR spectra of mel-C_{15} free in solution and within

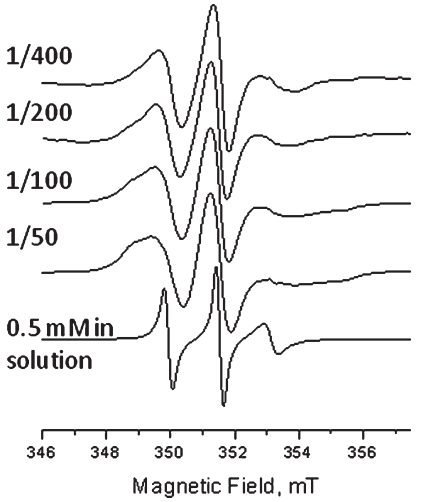

Figure 4. X-band CW EPR (303 K) spectra of mel-C_{15} in the absence and presence of LUVs at different P/PL.

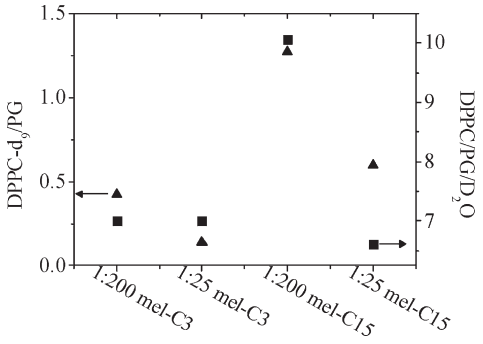

Figure 5. $I(^2H)$ values of mel-C_3 and mel-C_{15}, within DPPC-d_9/PG (triangles) and DPPC/PG/D_2O (squares) at different P/PL.

LUVs at different P/PL (1/400, 1/200, 1/100, and 1/50). Similar to the phospholipid spin probes, a progressive increase in the width of the spectrum was observed as P/PL increased, indicating a restriction in the degree of motional freedom of the spin label.

The effect of P/PL on the melittin orientation and penetration depth into the LUVs was monitored by ESEEM measurement of mel-C_3 and mel-C_{15} in DPPC/PG/D_2O and DPPC-d_9/PG LUVs. The results are presented in Figure 5. The spin label in mel-C_{15} was found to be the most solvent exposed for low P/PL.[20] As the P/PL

dx.doi.org/10.1021/jp207159z |J. Phys. Chem. B 2012, 116, 179–188

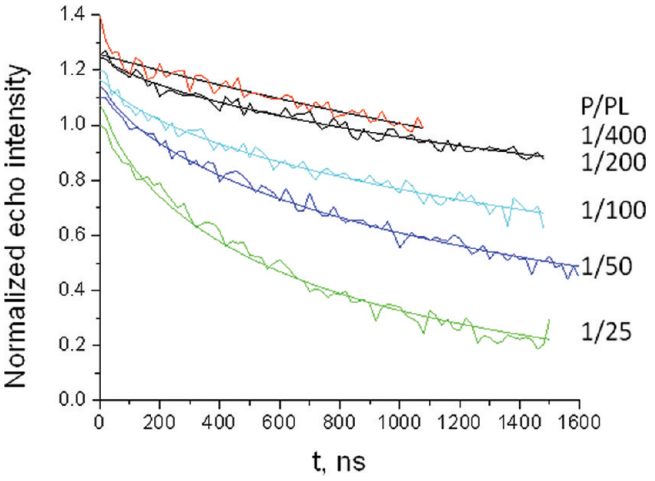

Figure 6. DEER traces obtained for mel-C_{15} within LUVs, at different P/PL ratios. The corresponding solid lines represent the fit with a dimensionality of 2 (d = 2). All traces were normalized to 1, and for clarity, each trace (except for the 1:25) was shifted vertically by 0.1 relative to the previous one.

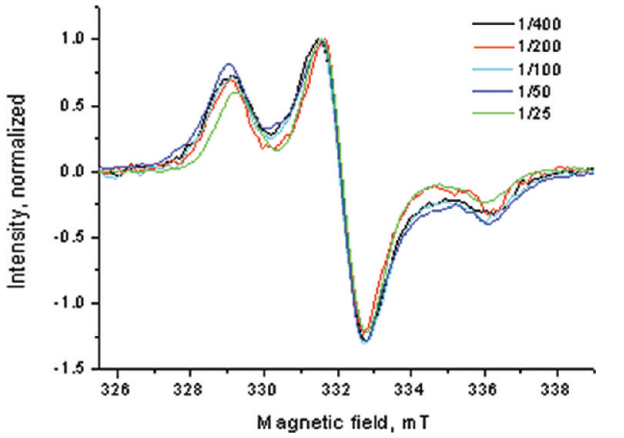

Figure 7. X-band CW EPR spectra of mel-C_{15} in the presence of LUVs at different P/PL ratios, measured at 130 K. The spectra were normalized to the central component.

increased from 1/200 to 1/25, a considerable decrease in $I(^2H)$ was observed for mel-C_{15} in both DPPC-d_9/PG and DPPC/PG/D_2O. The spin label in mel-C_3 was found to be deeper in the phospholipid layer than in mel-C_{15},[20] and in DPPC-d_9/PG, it exhibited some decrease in $I(^2H)$ as P/PL increased. This reflects a change in the ^2H density in the peptide's region. In contrast, no difference was found for mel-C_3 in the DPPC/PG/D_2O sample. These set of experiments indicate that the central region of melittin penetrated deeper into the membrane as the P/PL ratio increased.

To probe the presence of specific melittin aggregates that are expected to exist for the toroidal pores or the barrel-stave models, DEER measurements on mel-C_{15} in LUVs with different P/PL ratios were carried out. The results are shown in Figure 6. Due to the considerably higher local concentration of spins in LUVs solutions as compared to aqueous solutions without LUVs, it was difficult to acquire DEER traces with dipolar evolution times longer than 1.8 μs.[20,48] This time can be extended by using nanolipoprotein phospholipid bilayers, commonly referred to as nanodiscs;[18,49] we refrained from using this because we did not want to add another component to the system that may modify it. The time domain DEER data of all the mel-C_{15} in the LUVs samples showed a monotonous decay, not revealing any modulations characteristic of a specific inter spin distance. The DEER traces could be fitted with a homogeneous decay with a dimensionality, d = 2, as expected for a homogeneous distribution of spins in a membrane.[50] These results suggest that intermolecular distances in the range 1.7−4 nm are not present.[51] More detailed explanation and plots of the decay coefficients as a function of P/PL compared to aqueous solutions appear in the Supporting Information, Figures S1 and S2.

To probe the possible existence of shorter distances that cannot be detected by DEER, we looked for broadening in the CW EPR spectra of frozen LUVs with various P/PL ratios (see Figure 7). The spectra look very similar, except that of P/PL = 1/25, which exhibit a smaller A_{zz} value. Second moment analysis of the EPR spectra, with the spectrum of P/PL ratio of 1/400 representing the noncoupled spectrum, did not reveal distances that are shorter than 1.5 nm.[52−54]

According to a model reported earlier,[55,56] melittin forms tetramers, where the peptides are arranged according to their amphiphatic nature and form a channel in the membrane with spherical radius of 10 Å. Assuming that the channel is lined by the peptides and considering a melittin α helix diameter and the spin label tether length,[57] a distribution of distances with a maximum value of approximately 4.3 nm is expected. This is consistent with the size of melittin pore that has been estimated to be between 3.5 and 4.5 nm by TEM.[58] Such distances should have been detected by the DEER measurements, and their absence support the monomeric state though we cannot exclude the presence of nonspecific aggregates with distances larger than 5 nm between the spin labels.

DISCUSSION

Our experimental observations on the action of melittin on a model membrane focused at two levels, the mesoscale, that is, the size and shape of the vesicles, which was obtained from cryo-TEM, and the molecular level, obtained from a combination of EPR techniques. Cryo-TEM images taken 1 min after the addition of melittin revealed a large number of discs. Images of the same sample frozen 20 min after the addition of melittin showed much less discs. This indicated that melittin caused rupturing of the vesicles, which then reassociated into larger, ill-shaped vesicles. All EPR measurements were carried out on samples equilibrated for 20 min or more after the addition of melittin, namely, after the ruptured vesicles have reassembled or fused. We refer to this state as a new equilibrium state to distinguish it from the initial equilibrium state and the process of rupturing and fusion. Previous cryo-TEM measurements on DOPC and POPC liposomes with melittin and P/PL of 1/60 to 1/30 showed ruptured liposomes and occasionally also some fused liposomes were observed after 15 min.[47] Furthermore, a 90° laser scatter study performed on cells demonstrated vesicle formation within less than 2 min as a direct result of the action of melittin.[59] In principle, cryo-TEM could also provide information regarding changes in the membrane hydrophobic thickness;[60,61] however, we did not resolve such changes due to limited resolution. The reported change of ∼2 Å that is associated with membrane thinning[1,61] is beyond the resolution we obtained in the cryo-TEM images of the vesicles.

The EPR measurements focused on molecular level structural information of the melittin/DPPC/PG LUVs at the new equilibrium state (>20 min). They reported on changes

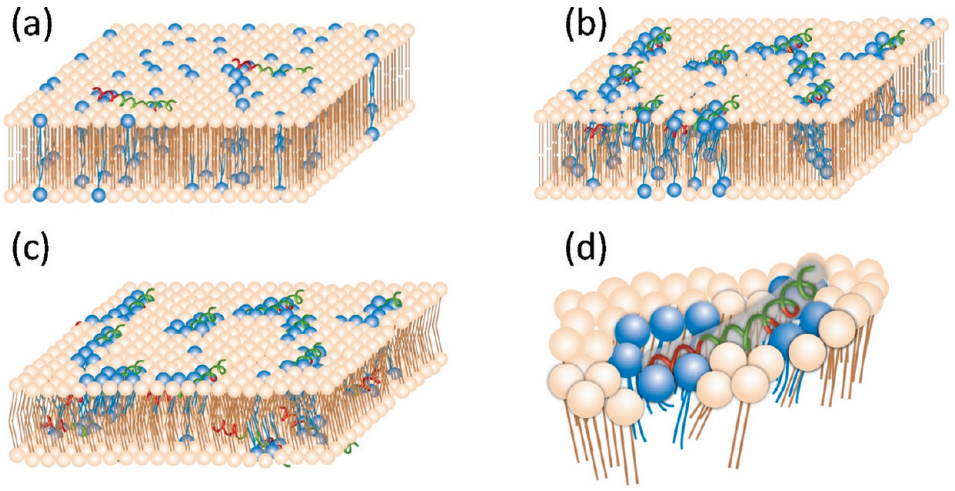

Figure 8. Schematic suggested model illustrating the melittin/DPPC/PG system that is consistent with the experimental results presented here and in our previous work.[20] (a) Melittin binds as a monomer in the outer membrane leaflet interacting preferentially with anionic PG molecules. The peptides are bound to the surface of the membrane their central hydrophilic residues facing the solvent and hydrophobic residues are in the hydrophobic region of the membrane. (b) PLs segregate and melittin penetrates deeper into the membrane core. (c) A membrane after disruption that allows the peptides to accumulate on both leaflets; alkyl chains are tilted. (d) Magnification of the peptide region illustrating the tilting of the alkyl chains in the vacant space under the peptide. Hydrophobic regions of the peptide are shown colored red, the hydrophilic regions are shown colored green, DPPC molecules appear in beige, and PG molecules are in blue.

occurring due to P/PL increase from 1/200 to 1/50 both for the peptide and the lipid bilayer. Specifically, we found that (i) melittin penetrated deeper into the lipid bilayer and became less mobile, and no specific aggregates of melittin (like tetramers) were detected and (ii) the changes in terms of local density of the DPPC lipids were opposite in the polar head and alkyl chain regions; it increased in the polar head region, and decreased in the alkyl chain part. The change in the water penetration depth was very mild, and a small increase was detected only in the polar head region. The mobility of the alkyl chains in the DPPC phospholipid environment decreased both in the upper part and the lower part. While in the cryo-TEM images we resolve single LUVs, the EPR measurements report on the properties averaged over all LUVs, those that have remained intact and those that ruptured and recombined. Based on EPR observations, we constructed a schematic structural model for the equilibrated melittin/DPPC/PG system that is presented in Figure 8 and is consistent with all our experimental observations as we discuss next.

Figure 8a represent the situation at low P/PL where melittin is mostly helical and parallel to the membrane surface[20] and the DPPC and PG phospholipids are mixed homogenously.[62] The increase in ^{2}H nuclei density sensed by HPCSP and 5PCSP in DPPC-d_9/PG LUVs with increasing P/PL indicates a closer packing of the DPPC head groups. Such a situation would arise from a partial insertion of the peptide into the lipid bilayer, thereby pushing away the lipid heads in the peptide region and causing their redistribution throughout the membrane. Naturally, when the number of peptides in the LUVs increases, this perturbation increases, and the overall change in the packing throughout the membrane becomes more substantial. Such a change is expected to be associated with a decrease in lipid mobility as well, as observed for 5PCSP. However, because melittin insertion is not transmembranal, the perturbation in the region of the alkyl chain is different than in the polar head region. In the alkyl chains region, the packing is expected to become looser because they can expand into the volume not occupied by the peptide. This is in line with reduced ^{2}H density of the alkyl chains as opposed to the increase in the polar head region but not with reduced mobility of 10PCSP. Therefore, additional effects should be considered.

The different changes in packing for the polar head and the alkyl chain regions may lead to changes in curvature and an overall thinning of the membrane even at low peptide concentration.[63] Recently, it has been reported that the addition of melittin to DOPC bilayers and to bilayers composed of two lipids of different chain lengths, 1,2-dierucoyl*sn*-glycero-3-phosphocholine (di22:1PC) and 1,2-dieicosenoyl*sn*-glycero-3-phosphocholine (di20:1PC), leads to thinning of the membrane.[1,61] The molecular basis for such a thinning has been attributed to volume conservation of the hydrocarbon chains, meaning that an expansion in the area due to peptide interaction is equivalent to a thinning of the membrane.[1] Thinning could be associated with a tilt of the alkyl chains, such that they adopt particular conformations to avoid leaving a vacant space in the middle of the bilayer under the peptide that is formed due to the disorder in the lipids upper layer (Figure 8c, d).[64] This change may lead to a reduced density of the alkyls chain while reducing their mobility toward the end of the chain as compared to unperturbed membrane.

The binding of positively charged peptides, such as melittin, can also be associated with preferred interaction of the anionic PG molecules,[23,65] thus leading to phospholipids segregation, forming regions around the peptide that are rich with PG and others, further away, rich with DPPC molecules (Figure 8b).[66,67] Because the spin-labeled phospholipids were of DPPC type (zwitterionic) and not of PG type, the segregation should be associated with an increase in the $I(^2H)$ density in both the polar head and alkyl chain region. Furthermore, the segregation should also lead to a better packing of the alkyl chains of the DPPC region because of the absence of the PG molecules, which have an unsaturated alkyl chain. This, in turn, should be reflected in the increased rigidity of 5PCSP and 10PCSP. Accordingly, both segregation and the change in the lipid organization/packing due

to partial insertion of melittin as discussed above should lead to increase in $I(^2H)$ in DPPC-d_9 of HPCSP and 5PCSP and to reduced mobility of 5PCSP, as observed experimentally. The situation is different when the alkyl chain region is concerned. While segregation is expected to increase $I(^2H)$ and decrease mobility, the partial insertion of the peptide has opposite effects. The latter should affect more the PG phospholipids that are closer to the peptide but is expected to be translated throughout the membrane. To account for the experimental results, we suggest that, while the segregation effect dominates in terms of the reduced mobility, the disorder in the alkyl chain induced by the partial insertion of the peptide dominates in terms of the DPPC ^2H density.

The segregation of lipids should bring about a decrease in $I(^2H)$ for both mel-C_3 and mel-C_{15} in DPPC-d_9/PG as indeed is observed, and therefore, this decrease cannot be used as an evidence for insertion into the membrane. The decrease in $I(^2H)$ observed for mel-C_{15} but not for mel-C_3 in DPPC/PG/D_2O indicates that the center part of the peptide penetrated deeper into the membrane. Accordingly, melittin changes its orientation with respect to membrane surface, becoming more tilted as the P/PL ratio increased to 1/25. Hence, the reduction in $I(^2H)$ for mel-C_{15} in DPPC-d_9/PG has also contributions from the deeper insertion into the membrane, in addition to the segregation. The associated reduced mobility of mel-C_{15} is consistent with a deeper insertion and the better interaction with the increased number of the negative PG lipids in its vicinity. Finally, the small increase in the $I(^2H)$ of HPCSP, but not for 5PCSP in DPPC/PG/D_2O, suggests some expulsion of the label at the polar head toward the water. This could be a consequence of its increased perturbation in the better ordered DPPC rich regions.

As the number of adsorbed melittin molecules increases, the perturbation induced by the peptide insertion and the lipid segregation, which initially occur at the upper leflet only, will eventually lead to membrane rupture, as observed by cryo-TEM. Under these conditions, some peptides can translocate to the inner leaflet, and a new stable equilibrium state is formed. In the newly formed vesicles, peptides are present on both inner and outer leaflets, the tension is released, and this is the situation we probed by EPR. In general, vesicle rupture was also observed in pure POPC and DOPC membranes,[47] namely, destabilization of membranes can occur without segregation.

Models such as "barrel-stave", "toroidal pore", and "carpet" were suggested for the mode of action of melittin.[23,29−31,68] In the barrel-stave[29,69] and the toroidal pore[58,70] models, the peptide spans the bilayer and aggregates to line the pore. The existence of these models is inconsistent with the reduction of the water content near mel-C_{15} with increasing P/PL ratio. In addition, the existence of such pores is inconsistent with the DEER data, which did not reveal specific aggregation. The latter should have been observed by DEER as recently demonstrated for spin-labeled fatty acids in small micelles.[71] We also did not observe pores in the cryo-TEM images, though these may be below the required resolution. According to the carpet model, the peptide covers the membrane surface in a "carpet"- like manner,[72,73] and at a threshold concentration of monomers, transient pores are formed in the membrane leading to complete membrane lysis.[74,75] Our results are inconsistent with this model due to the following reasons: (i) we detect membrane fusion even at low P/PL ratio such as 1/200, (ii) penetration of peptide into alkyl chain region is observed, and (iii) the cryo-TEM measurements showed that, rather than forming small bilayer particles due to membrane rupture, large vesicles formed, as fusion of two or more vesicles integrated into new stable structures, a short time after melittin addition.

In a recently proposed model termed "the interfacial activity model",[76] the peptide perturbs the well-defined hydrocarbon region of the membrane even at low peptide concentration, allowing peptides and lipids to translocate to the other side of the membrane without pore formation due to peptide self-assembly. The bilayer is deformed, and the hydrocarbon region is disrupted such that it intermingles with polar phospholipid headgroup moieties. The observed reduced density in the alkyl chain region and the absence of aggregation are consistent with this model.

Finally, we stress that the EPR measurements give information averaged over the whole sample and we know from the cryo-TEM measurements that even for P/PL = 1/25 not all LUVs underwent rupture. Hence, the changes observed appear milder than they actually are due to contributions from unaltered LUVs. Furthermore, our study focused on the final equilibrium state, and therefore, it cannot exclude the formation of transient pore structures formed by some dynamic disorder process.[70] Accordingly, further detailed characterization of the rupture mechanism should include time-resolved measurements.

CONCLUSIONS

The action of melittin on a negatively charged model membrane with emphasis on the effect of the melittin/phospholipids ratio was investigated on the molecular level using a combination of EPR techniques such as DEER, ESEEM, and CW EPR and on the mesoscale with cryo-TEM. We particularly note the ESEEM results that highlighted opposite perturbations in the phospholipids polar head and alkyl chain regions. It was found that melittin causes vesicles rupture and their reassembly into new larger vesicles. In this new state and at P/PL = 1/200, melittin bind to the membrane as isolated molecules lying on the surface of the membrane. As the P/PL ratio increases, melittin tilts and inserts deeper into the membrane causing a change in the distribution and mobility of the lipid polar head and alkyl region. This is possibly also associated with segregation of DPPC and PG lipids where the negatively charged PG lipids interact with the positively charged melittin. Our results do not rule out that transient pores were formed before the system reached the new equilibrium conditions.

ASSOCIATED CONTENT

Supporting Information. Brief summary of the DEER theory, the dependence of the exponential decay constant of the DEER traces of mel-C_{15} on P/PL (peptide concentration) compared to that of MTSL in a water glycerol solution, and the DEER traces obtained for different concentrations of MTSL in 30% glycerol/D_2O. This material is available free of charge via the Internet at http://pubs.acs.org.

AUTHOR INFORMATION

Corresponding Author
*E-mail: daniella.goldfarb@weizmann.ac.il.

ACKNOWLEDGMENT

The electron microscopy studies were conducted at the Irving and Cherna Moskowitz Center for Nano and Bio-Nano Imaging at the Weizmann Institute of Science. This work was supported

by the ISF-VATAT Converging Technologies Program and by the Minerva Foundation. D.G. holds the Erich Klieger Professorial Chair in Chemical Physics.

REFERENCES

(1) Chen, F. Y.; Lee, M. T.; Huang, H. W. *Biophys. J.* **2003**, *84*, 3751.
(2) Lam, Y. H.; Wassall, S. R.; Morton, C. J.; Smith, R.; Separovic, F. *Biophys. J.* **2001**, *81*, 2752.
(3) Lorigan, G. A.; Dave, P. C.; Tiburu, E. K.; Damodaran, K.; Abu-Baker, S.; Karp, E. S.; Gibbons, W. J.; Minto, R. E. *J. Am. Chem. Soc.* **2004**, *126*, 9504.
(4) Yamaguchi, S.; Hong, T.; Waring, A.; Lehrer, R. I.; Hong, M. *Biochemistry* **2002**, *41*, 9852.
(5) Hu, F.; Luo, W.; Hong, M. *Science* **2010**, *330*, 505.
(6) Levin, I. W.; Lavialle, F.; Mollay, C. *Biophys. J.* **1982**, *37*, 339.
(7) Hristova, K.; Dempsey, C. E.; White, S. H. *Biophys. J.* **2001**, *80*, 801.
(8) Hubbell, W. L.; Gross, A.; Langen, R.; Lietzow, M. A. *Curr. Opin. Struct. Biol.* **1998**, *8*, 649.
(9) Fanucci, G. E.; Cafiso, D. S. *Curr. Opin. Struct. Biol.* **2006**, *16*, 644.
(10) Nielsen, R. D.; Che, K.; Gelb, M. H.; Robinson, B. H. *J. Am. Chem. Soc.* **2005**, *127*, 6430.
(11) Hustedt, E. J.; Beth, A. H. Biological magnetic resonance: Structural information from CW-EPR spectra of dipolar coupled nitroxide spin labels. In *Distance Measurements in Biological Systems by EPR*; Berliner, L. J., Eaton, S. S., Eaton, G. R., Eds.; Kluwer Academic/Plenum Publishers: New York, 2000; Vol. 19, p 155.
(12) Han, X.; Bushweller, J. H.; Cafiso, D. S.; Tamm, L. K. *Nat. Struct. Biol.* **2001**, *8*, 715.
(13) Altenbach, C.; Greenhalgh, D. A.; Khorana, H. G.; Hubbell, W. L. *Proc. Natl. Acad. Sci. U.S.A.* **1994**, *91*, 1667.
(14) Milov, A. D.; Erilov, D. A.; Salnikov, E. S.; Tsvetkov, Y. D.; Formaggio, F.; Toniolo, C.; Raap, J. *Phys. Chem. Chem. Phys.* **2005**, *7*, 1794.
(15) Salnikov, E. S.; Erilov, D. A.; Milov, A. D.; Tsvetkov, Y. D.; Peggion, C.; Formaggio, F.; Toniolo, C.; Raap, J.; Dzuba, S. A. *Biophys. J.* **2006**, *91*, 1532.
(16) Milov, A. D.; Samoilova, R. I.; Tsvetkov, Y. D.; De Zotti, M.; Toniolo, C.; Raap, J. *J. Phys. Chem. B* **2008**, *112*, 13469.
(17) Drescher, M.; Veldhuis, G.; van Rooijen, B. D.; Milikisyants, S.; Subramaniam, V.; Huber, M. *J. Am. Chem. Soc.* **2008**, *130*, 7796.
(18) Georgieva, E. R.; Ramlall, T. F.; Borbat, P. P.; Freed, J. H.; Eliezer, D. *J. Am. Chem. Soc.* **2008**, *130*, 12856.
(19) Jao, C. C.; Hegde, B. G.; Chen, J.; Haworth, I. S.; Langen, R. *Proc. Natl. Acad. Sci. U.S.A.* **2008**, *105*, 19666.
(20) Gordon-Grossman, M.; Gofman, Y.; Zimmermann, H.; Frydman, V.; Shai, Y.; Ben-Tal, N.; Goldfarb, D. *J. Phys. Chem. B* **2009**, *113*, 12687.
(21) Habermann, E. *Science* **1972**, *177*, 314.
(22) Gauldie, J.; Hanson, J. M.; Rumjanek, F. D.; Shipolini, R. A.; Vernon, C. A. *Eur. J. Biochem.* **1976**, *61*, 369.
(23) van den Bogaart, G.; Guzman, J. V.; Mika, J. T.; Poolman, B. *J. Biol. Chem.* **2008**, *283*, 33854.
(24) Almeida, P. F.; Pokorny, A. *Biochemistry* **2009**, *48*, 8083.
(25) Carmieli, R.; Papo, N.; Zimmermann, H.; Potapov, A.; Shai, Y.; Goldfarb, D. *Biophys. J.* **2006**, *90*, 492.
(26) Kevan, L.; Schwartz, R. N. Modulation of electron spin-echo decay in solids. In *Time Domain Electron Spin Resonance*; John Wiley & Sons: New York, 1979; p 279.
(27) Milov, A. D.; Samoilova, R. I.; Tsvetkov, Y. D.; De Zotti, M.; Formaggio, F.; Toniolo, C.; Handgraaf, J. W.; Raap, J. *Biophys. J.* **2009**, *96*, 3197.
(28) Sevcsik, E.; Pabst, G.; Jilek, A.; Lohner, K. *Biochim. Biophys. Acta* **2007**, *1768*, 2586.
(29) Brogden, K. A. *Nat. Rev. Microbiol.* **2005**, *3*, 238.
(30) Allende, D.; Simon, S. A.; McIntosh, T. J. *Biophys. J.* **2005**, *88*, 1828.
(31) Yang, L.; Harroun, T. A.; Weiss, T. M.; Ding, L.; Huang, H. W. *Biophys. J.* **2001**, *81*, 1475.
(32) Ge, M.; Freed, J. H. *Biophys. J.* **2009**, *96*, 4925.
(33) Eibl, H. *Proc. Natl. Acad. Sci. U.S.A.* **1978**, *75*, 4074.
(34) Fellmann, P.; Zachowski, A.; Devaux, P. F. *Methods Mol. Biol.* **1994**, *27*, 161.
(35) MacDonald, R. C.; MacDonald, R. I.; Menco, B. P.; Takeshita, K.; Subbarao, N. K.; Hu, L. R. *Biochim. Biophys. Acta* **1991**, *1061*, 297.
(36) Jeschke, G.; Wegener, C.; Nietschke, M.; Jung, H.; Steinhoff, H. J. *Biophys. J.* **2004**, *86*, 2551.
(37) Upadhyay, A. K.; Borbat, P. P.; Wang, J.; Freed, J. H.; Edmondson, D. E. *Biochemistry* **2008**, *47*, 1554.
(38) Anchordoguy, T. J.; Rudolph, A. S.; Carpenter, J. F.; Crowe, J. H. *Cryobiology* **1987**, *24*, 324.
(39) Ghimire, H.; McCarrick, R. M.; Budil, D. E.; Lorigan, G. A. *Biochemistry* **2009**, *48* (25), 5782.
(40) Bellare, J. R.; Davis, H. T.; Scriven, L. E.; Talmon, Y. *J. Electron. Microsc. Tech.* **1988**, *10*, 87.
(41) Fauth, J. M.; Schweiger, A.; Braunschweiler, L.; Forrer, J.; Ernst, R. R. *J. Magn. Reson.* **1986**, *66*, 74.
(42) Van Doorslaer, S.; Sierra, G. A.; Schweiger, A. *J. Magn. Reson.* **1999**, *136*, 152.
(43) Erilov, D. A.; Bartucci, R.; Guzzi, R.; Shubin, A. A.; Maryasov, A. G.; Marsh, D.; Dzuba, S. A.; Sportelli, L. *J. Phys. Chem. B* **2005**, *109*, 12003.
(44) Pannier, M.; Veit, S.; Godt, A.; Jeschke, G.; Spiess, H. W. *J. Magn. Reson.* **2000**, *142*, 331.
(45) Jeschke, G.; Chechik, V.; Ionita, P.; Godt, A.; Zimmermann, H.; Bahman, J.; Timmel, C. R.; Hilger, D.; Jung, H. *Appl. Magn. Reson.* **2006**, *30* (3−4), 473.
(46) Bradrick, T. D.; Philippetis, A.; Georghiou, S. *Biophys. J.* **1995**, *69*, 1999.
(47) Wessman, P.; Stromstedt, A. A.; Malmsten, M.; Edwards, K. *Biophys. J.* **2008**, *95*, 4324.
(48) Ruthstein, S.; Potapov, A.; Raitsimring, A. M.; Goldfarb, D. *J. Phys. Chem. B* **2005**, *109*, 22843.
(49) Zou, P.; McHaourab, H. S. *Biophys. J.* **2010**, *98*, L18.
(50) Hilger, D.; Jung, H.; Padan, E.; Wegener, C.; Vogel, K. P.; Steinhoff, H. J.; Jeschke, G. *Biophys. J.* **2005**, *89*, 1328.
(51) Jeschke, G.; Polyhach, Y. *Phys. Chem. Chem. Phys.* **2007**, *9*, 1895.
(52) Fanucci, G. E.; Coggshall, K. A.; Cadieux, N.; Kim, M.; Kadner, R. J.; Cafiso, D. S. *Biochemistry* **2003**, *42*, 1391.
(53) Gross, A.; Columbus, L.; Hideg, K.; Altenbach, C.; Hubbell, W. L. *Biochemistry* **1999**, *38*, 10324.
(54) Banham, J. E.; Baker, C. M.; Ceola, S.; Day, I. J.; Grant, G. H.; Groenen, E. J.; Rodgers, C. T.; Jeschke, G.; Timmel, C. R. *J. Magn. Reson.* **2008**, *191*, 202.
(55) Liu, P.; Huang, X.; Zhou, R.; Berne, B. J. *Nature* **2005**, *437*, 159.
(56) Vogel, H.; Jahnig, F. *Biophys. J.* **1986**, *50*, 573.
(57) Kensch, O.; Restle, T.; Wohrl, B. M.; Goody, R. S.; Steinhoff, H. J. *J. Mol. Biol.* **2000**, *301*, 1029.
(58) Park, S. C.; Kim, J. Y.; Shin, S. O.; Jeong, C. Y.; Kim, M. H.; Shin, S. Y.; Cheong, G. W.; Park, Y.; Hahm, K. S. *Biochem. Biophys. Res. Commun.* **2006**, *343*, 222.
(59) Weston, K. M.; Alsalami, M.; Raison, R. L. *Cytometry* **1994**, *15*, 141.
(60) Beck, P.; Liebi, M.; Kohlbrecher, J.; Ishikawa, T.; Ruegger, H.; Zepik, H.; Fischer, P.; Walde, P.; Windhab, E. *J. Phys. Chem. B* **2010**, *114*, 174.
(61) Lee, M. T.; Hung, W. C.; Chen, F. Y.; Huang, H. W. *Proc. Natl. Acad. Sci. U.S.A.* **2008**, *105*, 5087.
(62) Beschiaschvili, G.; Seelig, J. *Biochemistry* **1990**, *29*, 52.
(63) Heller, W. T.; Waring, A. J.; Lehrer, R. I.; Harroun, T. A.; Weiss, T. M.; Yang, L.; Huang, H. W. *Biochemistry* **2000**, *39*, 139.
(64) Berneche, S.; Nina, M.; Roux, B. *Biophys. J.* **1998**, *75*, 1603.
(65) Stromstedt, A. A.; Wessman, P.; Ringstad, L.; Edwards, K.; Malmsten, M. *J. Colloid Interface Sci.* **2007**, *311*, 59.
(66) Batenburg, A. M.; van Esch, J. H.; Leunissen-Bijvelt, J.; Verkleij, A. J.; de Kruijff, B. *FEBS Lett.* **1987**, *223*, 148.

(67) Faucon, J. F.; Bernard, E.; Dufourcq, J.; Pezolet, M.; Bougis, P. *Biochimie* **1981**, *63*, 857.
(68) Mihajlovic, M.; Lazaridis, T. *Biochim. Biophys. Acta* **2010**, *1798*, 1485.
(69) Tosteson, M. T.; Tosteson, D. C. *Biophys. J.* **1981**, *36*, 109.
(70) Sengupta, D.; Leontiadou, H.; Mark, A. E.; Marrink, S. J. *Biochim. Biophys. Acta* **2008**, *1778*, 2308.
(71) Bode, B. E.; Dastvan, R.; Prisner, T. F. *J. Magn. Reson.* **2011**, *211*, 11.
(72) Shai, Y. *Biopolymers* **2002**, *66*, 236.
(73) Shai, Y.; Oren, Z. *Peptides* **2001**, *22*, 1629.
(74) Gazit, E.; Boman, A.; Boman, H. G.; Shai, Y. *Biochemistry* **1995**, *34*, 11479.
(75) Shai, Y. *Trends Biochem. Sci.* **1995**, *20*, 460.
(76) Wimley, W. C. *ACS Chem. Biol.* **2010**, *5*, 905.